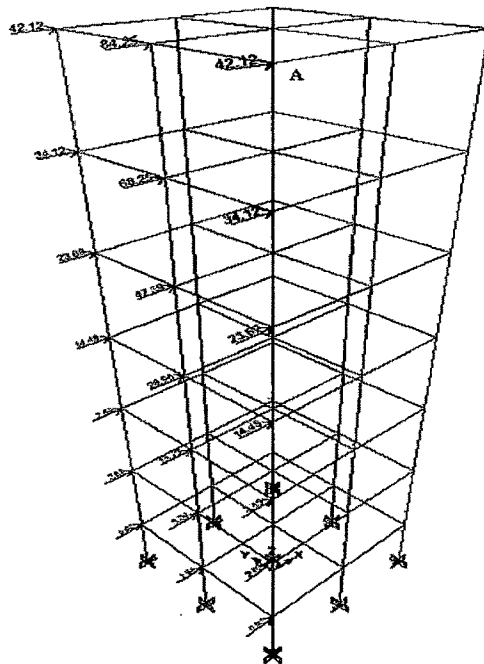


## CHAPTER 9

### EFFECT OF SEMIRIGIDITY OF JOINT ON SEISMIC PERFORMANCE OF RC SPACE FRAMES

#### 9.1 INCORPORATING SEMIRIGID JOINTS IN A SPACE FRAME

To investigate the behavior of semi rigid joints further, a seven storey RC space frame with two bays in each lateral directions of 3m x 3m panel size is studied in the present chapter for the effects of varying the rigidity of the beam to column joints under lateral loads. The normal gravity loads in the form of dead and live loads are applied on the frame. The earthquake loads are also applied as per IS 1893, Part 1, 2002 [24] as shown in **Fig. 9.1**. A point 'A' shown in the figure, at the end of a beam on the roof level is identified to study the changes in the bending moments developed due to variation in the stiffness of the beam to column joint.



**Fig. 9.1 G+6 Space Frame with Earthquake Loads in X-Direction**

The bending moments at point 'A' due to earthquake and live load cases are tabulated for varying the flexural stiffness of the end of all beams from 0 kNm/rad (pinned condition) to 10,00,000 kNm/rad (rigid condition) in **Table 9.1**.

**Table 9.1 Moments at Point A and Time Period for Varying Stiffness**

Joint Stiffness (kNm/rad)	BM due to EQ load (kNm)	BM due to Live load (kNm)	Fundamental Time Period (sec)
0	0.00	0.00	5.58
200	24.09	0.02	3.74
500	40.63	0.04	2.88
3000	54.72	0.21	1.59
20000	38.63	0.82	0.86
50000	33.05	1.16	0.72
75000	31.48	1.28	0.69
100000	30.63	1.35	0.67
125000	30.10	1.4	0.66
150000	29.74	1.43	0.65
175000	29.47	1.46	0.65
225000	29.11	1.49	0.64
300000	28.78	1.52	0.63
400000	28.53	1.54	0.63
500000	28.37	1.55	0.63
600000	28.28	1.56	0.62
750000	28.17	1.57	0.62
850000	28.13	1.58	0.62
1000000	28.07	1.58	0.62
Full Rigidity	27.57	1.67	0.61

**Table 9.1** also shows the changes in the fundamental time period of the building as the stiffness of the joints changes. The results obtained by analyzing the structure in SAP2000 are also depicted in a graphical form in **Fig. 9.2**. The moments at joint 'A' at the roof level shown in **Table 9.1** are plotted for live load and the earthquake load case on the same plot for comparison purpose in **Fig. 9.2**. The variation in the fundamental time period with change in the joint rigidity is plotted in **Fig. 9.3**.

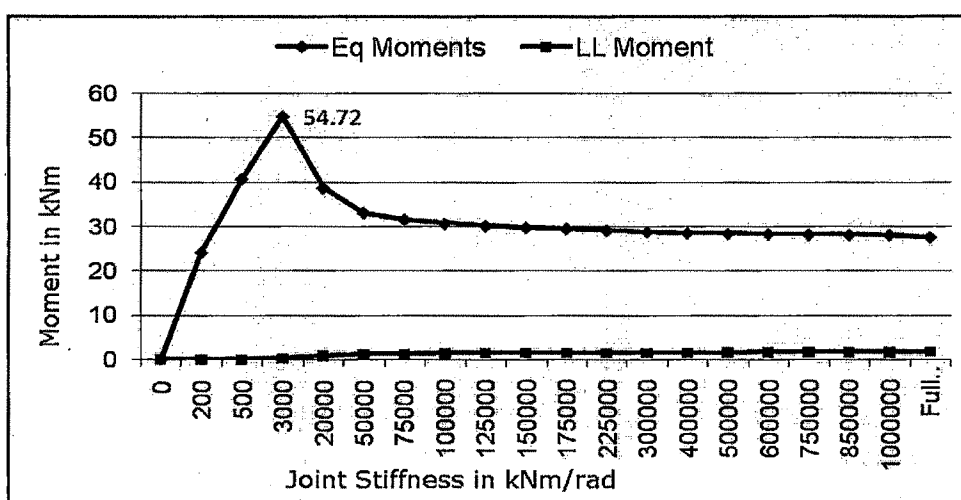


**Fig. 9.2 Variation of EQ and LL Moment with Joint Stiffness**

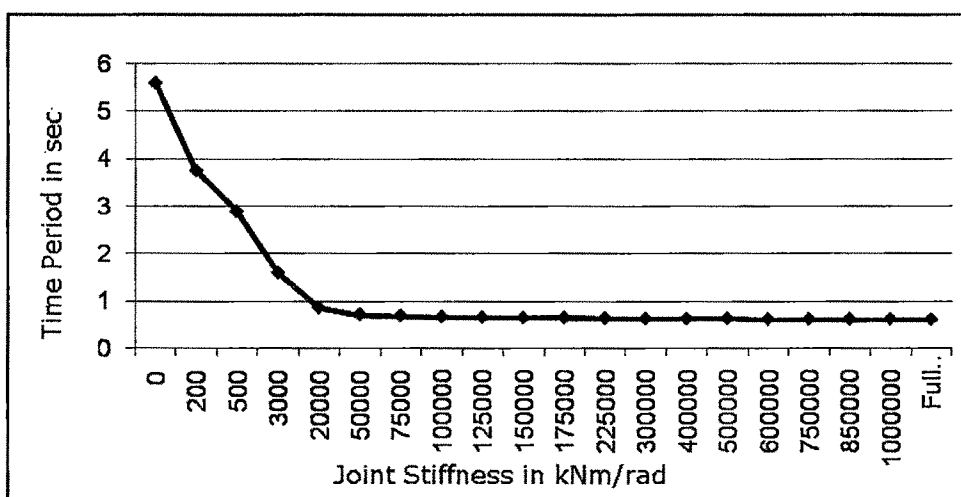


**Fig. 9.3 Variation of Fundamental Time Period with Joint Stiffness**

It can be observed from **Fig. 9.2** that the bending moment at end 'A' of the roof level beam rises monotonically with increase in end rigidity for gravity loads (Live load in this case). But, when one looks at the behavior of the same under earthquake loads, the moment rises with increase in the stiffness from zero to about 3000 kNm/rad reaching a peak value of 54.72 kNm and then starts decreasing as the rigidity increases. The moment at the end 'A' works out to be 27.57 kNm when all the joints are considered fully rigid, which is almost half of the peak moment observed at a joint rigidity of 3000 kNm/rad. There is a considerable variation in the fundamental time period of the building when the joints are considered as semi rigid instead of fully rigid. This fact is clearly indicated in **Fig. 9.3**. The peak value of moment obtained for semi rigid joints under lateral loads is instrumental in initiating further work on studying the effects of joint rigidity on earthquake moments developed in a space frame with varying floors and bays.

## 9.2 SEMIRIGIDITY IN SPACE FRAMES WITH VARYING STOREYS

Based on the above observations, mathematical models for RC space frames with G+2 storey to G+8 storey are developed and analyzed. The overall plan dimensions chosen are 6m x 6m with four panels of 3m x 3m in plan at each storey as shown in **Fig. 9.4**.

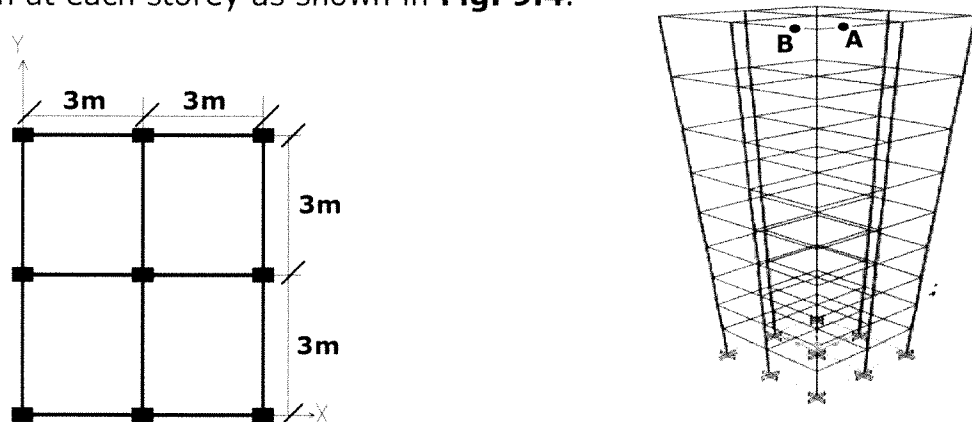


**Fig. 9.4 Typical Plan and Isometric View of the Model Considered**

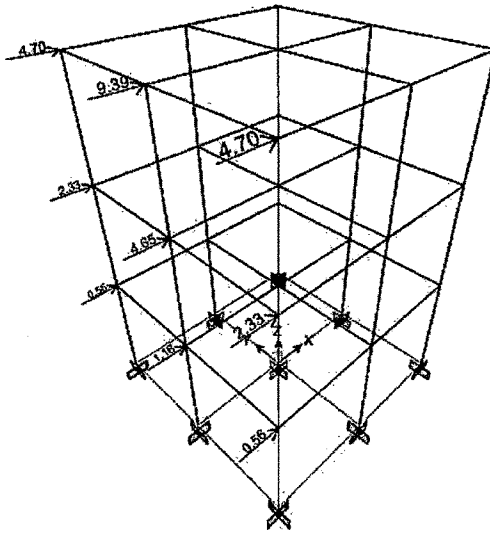


**Fig. 9.5 G+2 Frame with Earthquake Loads in X Direction**

**Table 9.2 Moments at Points A and B for Varying Stiffness**

<b>Joint Stiffness (kNm/rad)</b>	<b>Moment at A due to EqX (kNm)</b>	<b>Moment at B due to EqY (kNm)</b>
0	0.00	0.00
100	0.15	0.46
200	0.28	0.84
1000	1.12	2.32
2000	1.76	2.90
3000	2.17	3.13
5000	2.65	3.27
6000	2.80	3.28
7000	2.91	<b>3.29</b>
9000	3.06	3.28
10000	3.11	3.27
20000	3.28	3.18
30000	<b>3.29</b>	3.12
50000	3.25	3.07
60000	3.22	3.05
70000	3.20	3.04
75000	3.20	3.03
100000	3.16	3.02
Fully Rigid	3.01	2.96

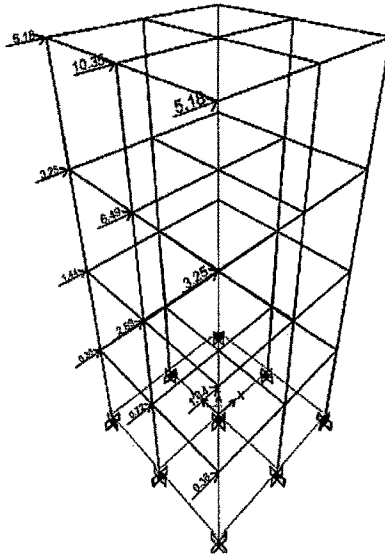


**Fig. 9.6 G+3 Frame With Earthquake Loads in X Direction**

**Table 9.3 Moments at Points A and B for Varying Stiffness in G+3**

<b>Joint Stiffness (kNm/rad)</b>	<b>Moment at A due to EqX (kNm)</b>	<b>Moment at B due to EqY (kNm)</b>
0	0.00	0.00
100	0.36	1.10
200	0.67	1.85
1000	2.31	3.90
2000	3.27	4.28
3000	3.75	<b>4.30</b>
5000	4.16	4.17
6000	4.25	4.10
7000	4.31	4.04
10000	<b>4.35</b>	3.88
20000	4.20	3.63
30000	4.04	3.53
50000	3.86	3.43
60000	3.80	3.41
70000	3.75	3.39
75000	3.73	3.38
100000	3.66	3.36
Fully Rigid	3.39	3.28

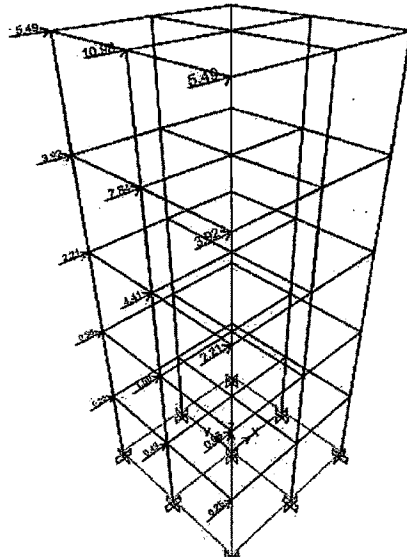


**Fig. 9.7 G+4 Frame With Earthquake Loads in X Direction**

**Table 9.4 Moments at Point A and B for Varying Stiffness in G+4**

<b>Joint Stiffness (kNm/rad)</b>	<b>Moment at A due to EqX (kNm)</b>	<b>Moment at B due to EqY (kNm)</b>
0	0.00	0.00
100	0.70	2.04
200	1.28	3.19
1000	3.77	<b>6.48</b>
2000	4.84	5.31
3000	5.24	5.09
5000	<b>5.43</b>	4.72
6000	5.42	4.59
7000	5.39	4.48
10000	5.23	4.25
20000	4.78	3.91
30000	4.51	3.78
50000	4.23	3.67
60000	4.15	3.64
75000	4.06	3.61
100000	3.96	3.58
Fully Rigid	3.64	3.49

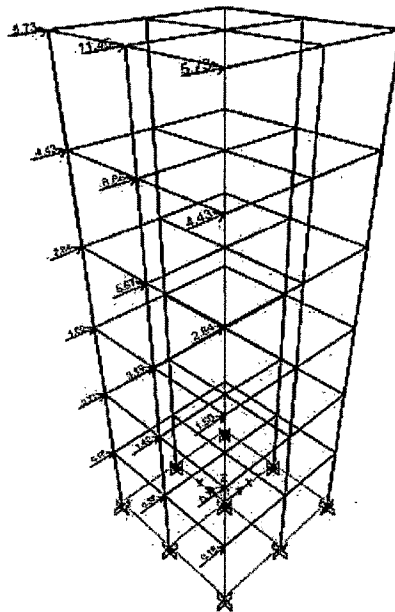


**Fig. 9.8 G+5 Frame With Earthquake Loads in X Direction**

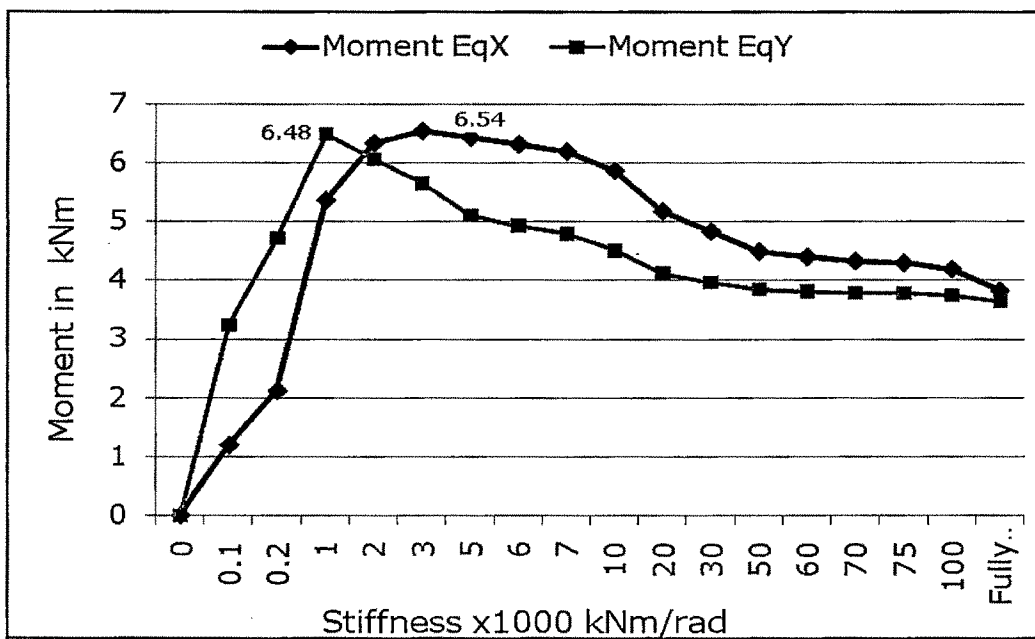


**Fig. 9.9 Moments at A and B for G+5 Frame for Varying Rigidity**



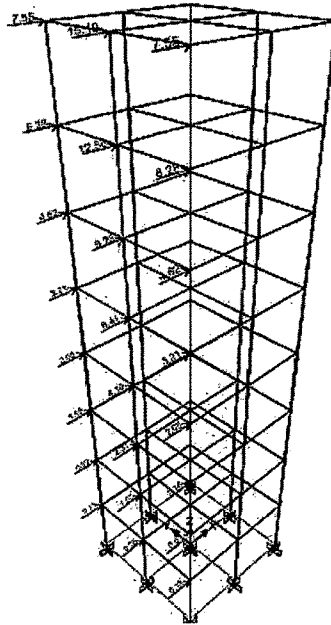


**Fig. 9.12 G+7 Frame with Earthquake Loads in X Direction**

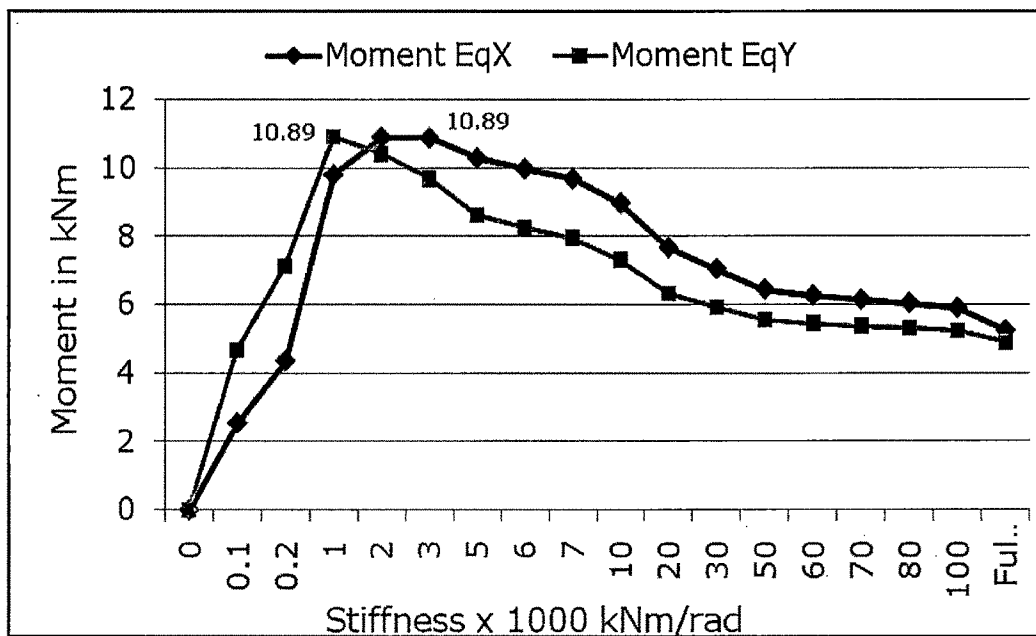


**Fig. 9.13 Moments at A and B for G+7 Frame for Varying Rigidity**



### 9.3 SUMMARY OF RESULTS

All the results are summarized in **Table 9.5** which represents the peak earthquake moments at point A for all the stories under varying rigidity of the beam ends. The shaded values are the moments which exceed the moment due to fully rigid joints. **Table 9.6** presents the summary in the form of ratio of peak moments at point A to the fully rigid moment when the models are subjected to earthquake force in the X-direction.

Similarly, **Table 9.7** presents peak earthquake moments at point B for all the stories under varying rigidity of all the beam ends when the models are subjected to earthquake load in Y-direction. The value of moments which exceed the fully rigid moments are shown by shading in the table. The ratio of peak moments to fully rigid moments is presented for all the models in **Table 9.8**.

**Table 9.5 Moments at Point A due to Earthquake Force in X dir.**

Storey	Highest Earthquake Moment under Varying Rigidity						
	3	4	5	6	7	8	9
9th							10.36
8th						10.89	11.21
7th					7.65	12.34	14.33
6th				6.54	8.87	16.74	18.31
5th			5.43	8.36	13.05	20.86	21.21
4th		4.35	7.80	12.16	16.00	23.66	23.16
3rd	3.29	7.04	10.98	14.51	17.76	25.26	24.26
2nd	5.85	9.30	12.44	15.43	18.31	25.34	24.18
1st	5.62	7.83	9.96	12.07	14.15	18.95	19.57



**Table 9.6 Ratio of Earthquake Moments at Point A - Force in X dir.**

Storey	Ratio of Peak Moment to Fully Rigid Moment						
	3	4	5	6	7	8	9
9th							2.39
8th						2.08	1.21
7th					1.94	1.11	NA
6th				1.71	1.01	NA	NA
5th			1.49	NA	NA	NA	NA
4th		1.28	NA	NA	NA	NA	NA
3rd	1.10	NA	NA	NA	NA	NA	NA
2nd	NA	NA	NA	NA	NA	NA	NA
1st	NA	NA	NA	NA	NA	NA	NA

**Table 9.7 Moments at Point B due to Earthquake Force in Y dir.**

Storey	Highest Earthquake Moment under Varying Rigidity						
	3	4	5	6	7	8	9
9th							10.33
8th						10.89	11.19
7th					7.41	12.16	15.37
6th				7.40	8.81	17.62	19.61
5th			6.48	9.19	14.38	21.93	22.67
4th		4.30	8.62	13.42	17.58	24.84	24.73
3rd	3.29	7.85	12.18	16.00	19.53	26.58	25.97
2nd	6.75	10.58	14.04	17.34	20.54	27.26	26.49
1st	7.14	9.85	12.48	15.10	17.69	22.14	23.73

**Table 9.8 Ratio of Earthquake Moments at point B - Force in Y dir.**

Storey	Ratio of Peak Moment to Fully Rigid Moment						
	3	4	5	6	7	8	9
9th							2.66
8th						2.23	1.14
7th					1.97	1.04	NA
6th				1.92	0.92	NA	NA
5th			1.86	NA	NA	NA	NA
4th		1.31	NA	NA	NA	NA	NA
3rd	1.11	NA	NA	NA	NA	NA	NA
2nd	NA	NA	NA	NA	NA	NA	NA
1st	NA	NA	NA	NA	NA	NA	NA

#### **9.4 SEISMIC PERFORMANCE OF SEMIRIGID SPACE FRAMES**

As can be seen from the analysis of RC space frames with semi rigid joints when subjected to lateral earthquake forces shows a peak moment. This phenomenon is further investigated here by subjecting the RC space frames to pushover analysis with beams having semi rigid ends corresponding to the peak moments exhibited. For example, referring to **Fig. 9.15**, for the G+8 storey space frame, peak moment is exhibited at a joint rigidity of 3000 kNm/rad when X direction forces are applied and 1000 kNm/rad when Y direction forces are applied. This fact is used in developing a G+8 storey semi rigid model with joint rigidity of 3000 kNm/rad which is subjected to X direction push. Similarly, the G+8 storey model having joint rigidity of 1000 kNm/rad is subjected to the Y directional push. The results obtained for push over analysis of semi rigid frame models are compared to those obtained by considering a model having all joints as fully rigid. This procedure is followed for all the space frame models with G+2 to G+8 storey.

The push over analysis is done using ETABS software and the following pushover cases are defined. PUSH1 is the gravity direction push which starts from zero initial conditions and ends when full intensity of the gravity loads is applied in the vertical direction. The default PMM plastic hinges are defined at the ends of all beams and columns. A roof level node is identified to monitor the push over cases. PUSHX is the pushover case defined in the lateral X direction which is applied as per the earthquake loads in the X direction and this case starts from the end of PUSH1 i.e. the gravity load push. The roof level node is monitored as per displacement control where the target displacement is given as 0.04 times the height of the building. PUSHY is another pushover case defined in the lateral Y direction and it is similar to PUSHX except that it is in the other lateral

direction. The plastic hinges which develop step wise under these push are monitored and effective damping and time period are recalculated at each step as per the provisions of ATC40 [1]. The P- $\Delta$  effect is considered for geometric non linearity and the building is considered to be of type B with medium soil. Taking these parameters into consideration, the performance point is evaluated for each of the building frames. The roof displacement and the base shear at the performance point are noted and are compared with those obtained for the same model with all the joints considered as fully rigid. The results of push over analysis for all the above models are presented in the form of deformed shape with colour coded hinges for PUSHX and PUSHY followed by the capacity versus demand spectra in ADRS format. A typical plot consists of demand and capacity spectrum superimposed along with a family of demand spectra for 5, 10, 15 and 20 percent damping.

**Figures 9.16, 9.19, 9.22, 9.25, 9.28, 9.31 and 9.34** represent the deformed shape of the semi rigid models at performance point under push in X and Y directions. The figures also indicate the developed hinges with colour coding indicating the severity of the hinges. **Figures 9.17, 9.20, 9.23, 9.26, 9.29, 9.32 and 9.35** present the demand versus capacity spectra in the ADRS format for the semi rigid models pushed in the X and Y directions for G+8 to G+2 frames. The comparison of the ADRS plots for the semi rigid frames is done with the same frames having fully rigid joints. The demand versus capacity curves plotted in the ADRS format for obtaining the performance point for fully rigid G+8 to G+2 storey frames are presented in **Figs. 9.18, 9.21, 9.24, 9.27, 9.30, 9.33 and 9.36**.

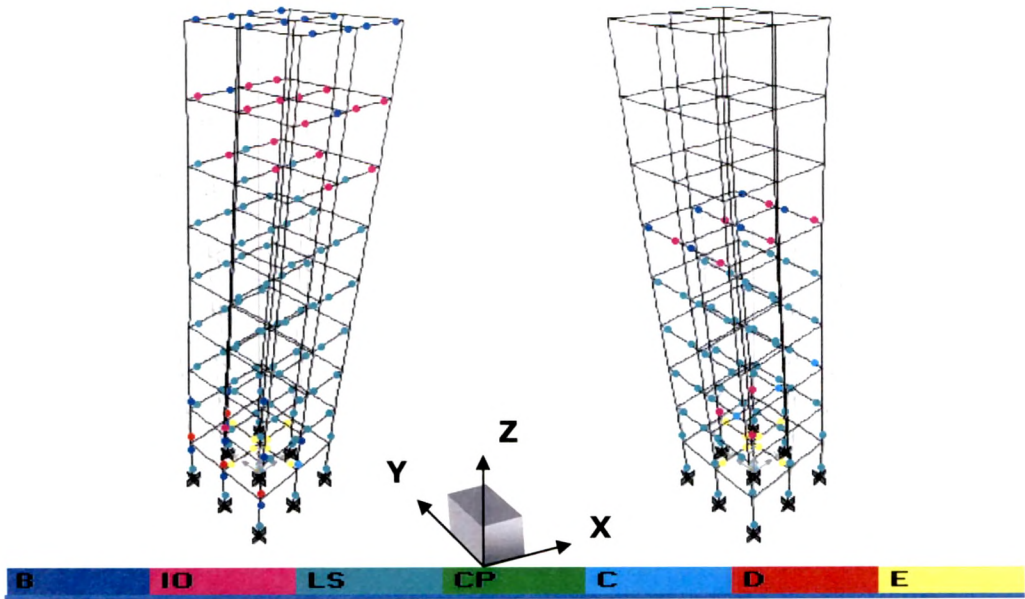


**Fig. 9.16 G+8 Frame with Semirigid Joints under Push PX and PY**

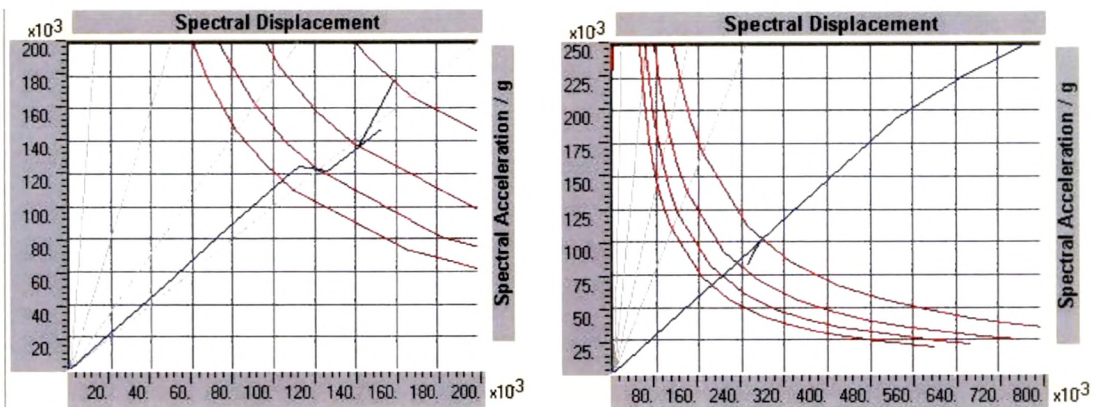


**Fig. 9.17 ADRS Plots - 3000 kNm/rad PX and 1000 kNm/rad PY**

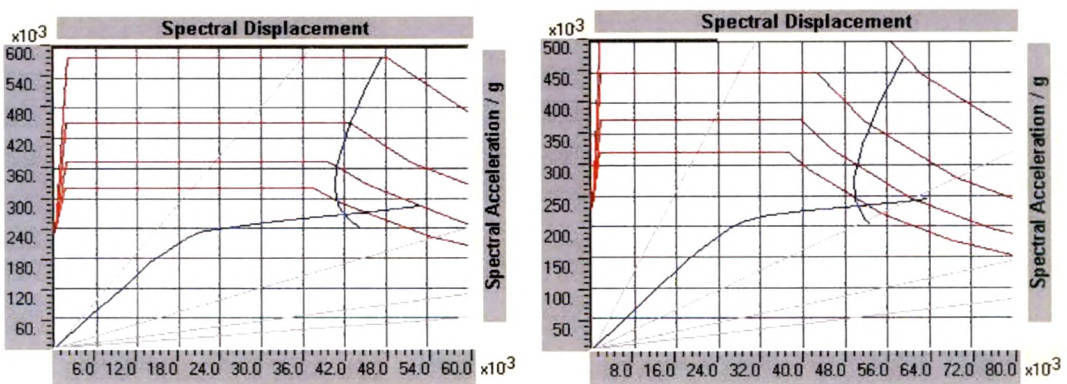
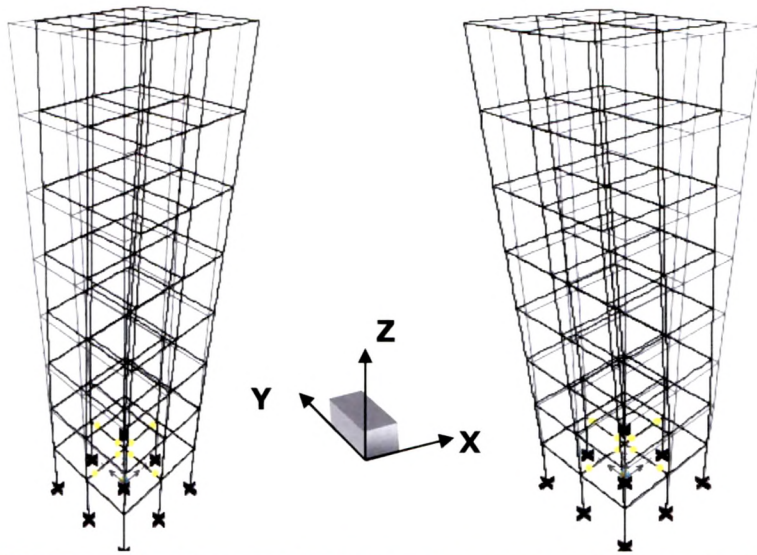


**Fig. 9.18 G+8 Frame ADRS Plots with Full Rigidity PX and PY**



**B IO LS CP C D E**  
**Fig. 9.19 G+7 Frame with Semirigid Joints under PUSH X and Y**

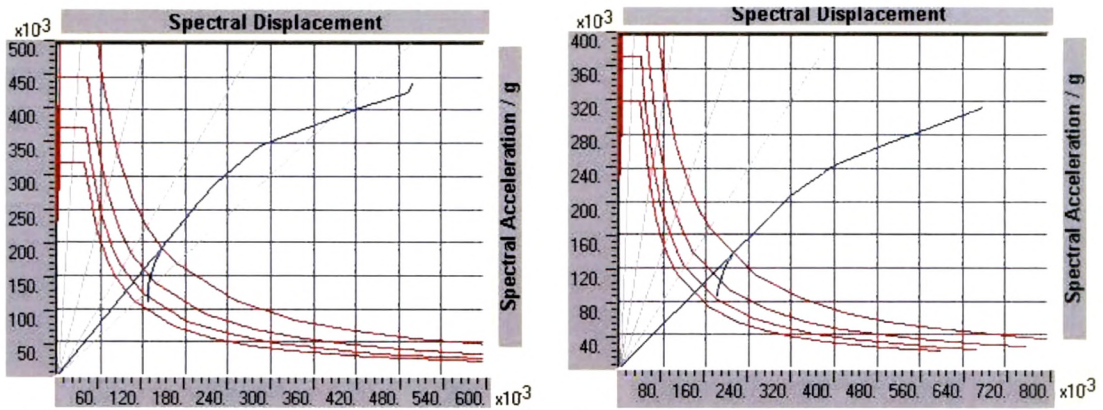


**Fig. 9.20 ADRS Plots – 2000 kNm/rad PX and 1000 kNm/rad PY**

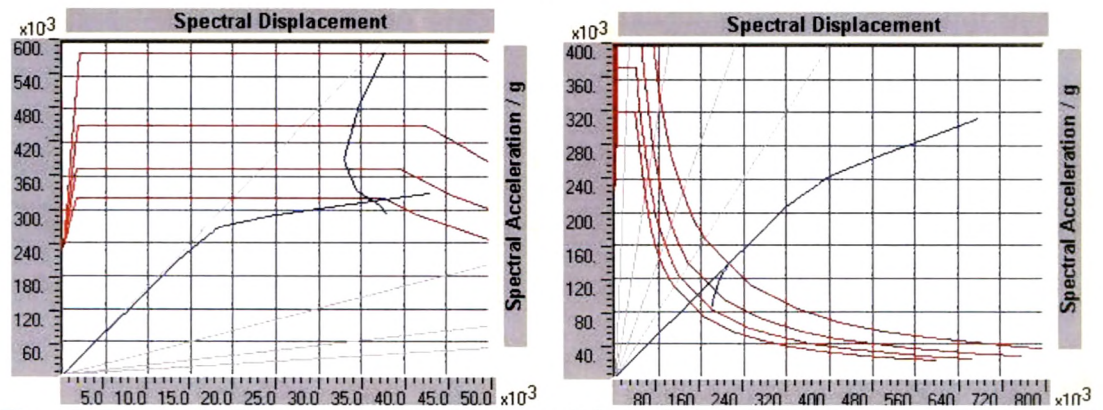


**Fig. 9.21 G+7 Frame ADRS Plots with Full Rigidity under PX and PY**

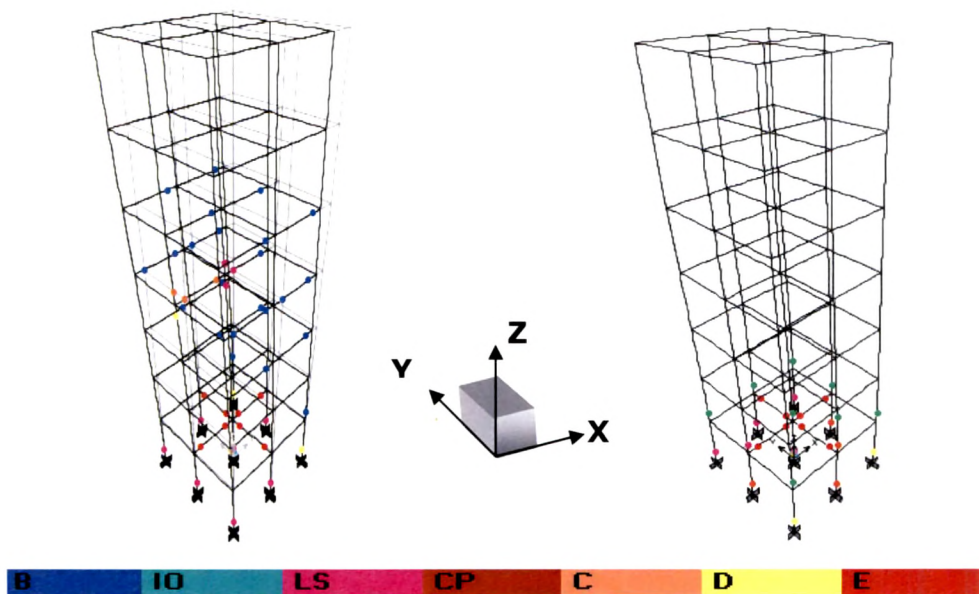


**Fig. 9.22 G+6 Frame with Semirigid Joints under PUSH X and Y**

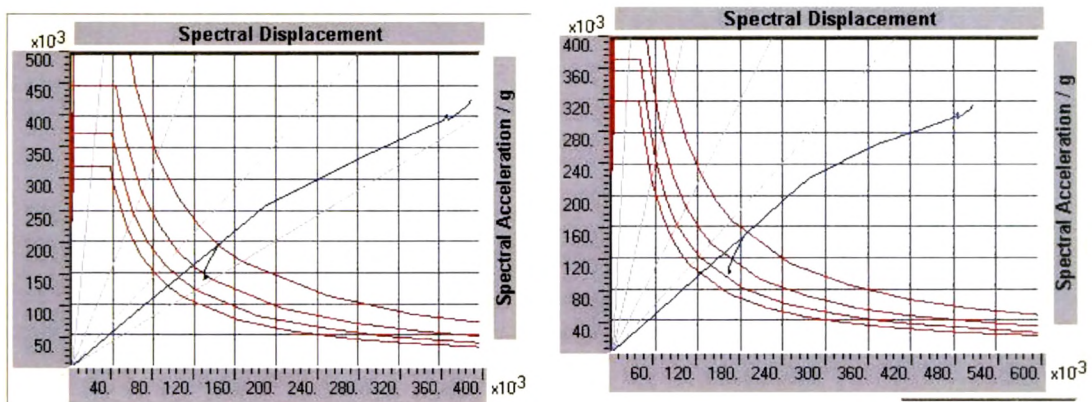


**Fig. 9.23 ADRS Plots – 2000 kNm/rad PX and 1000 kNm/rad PY**

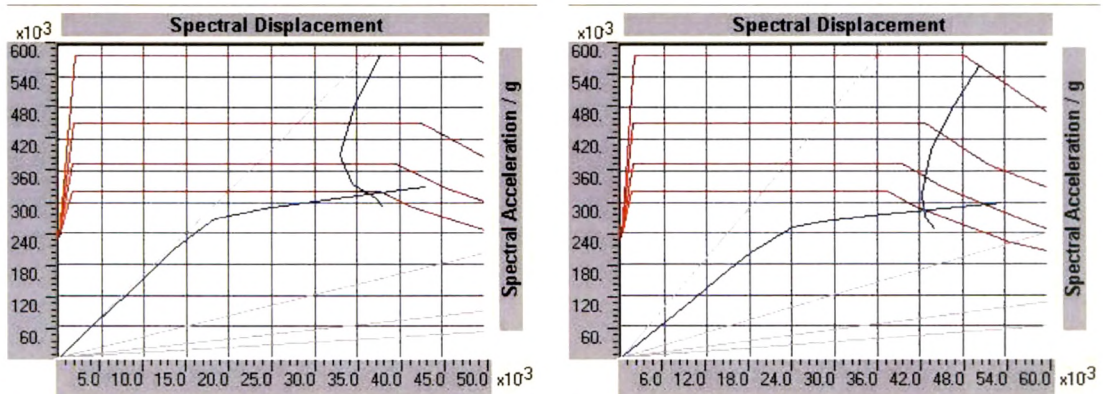


**Fig. 9.24 G+6 Frame ADRS Plots with Full Rigidity under PX and PY**

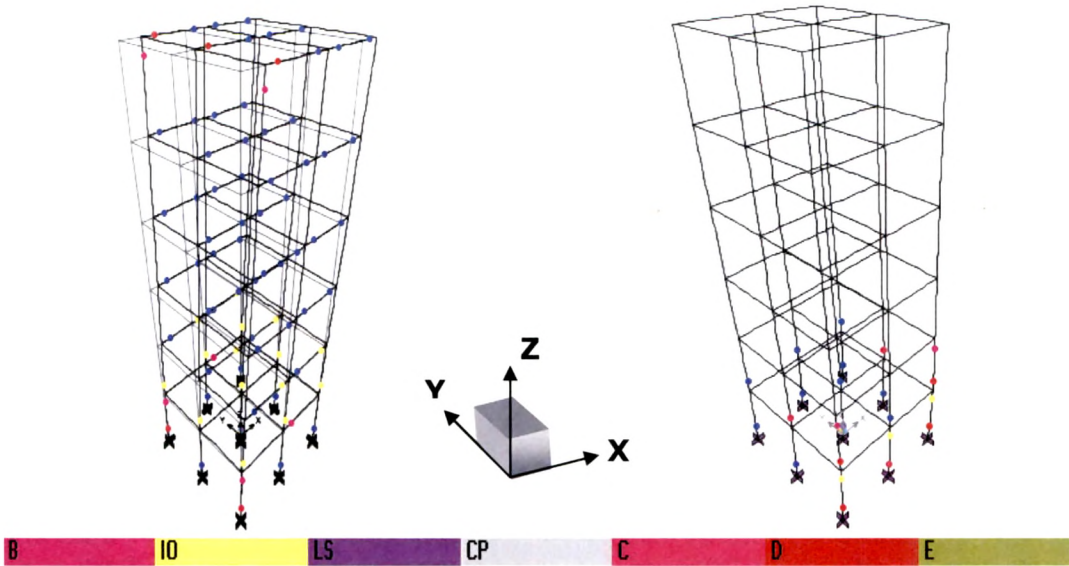


**Fig. 9.25 G+5 Frame with Semirigid Joints under PUSH X and Y**

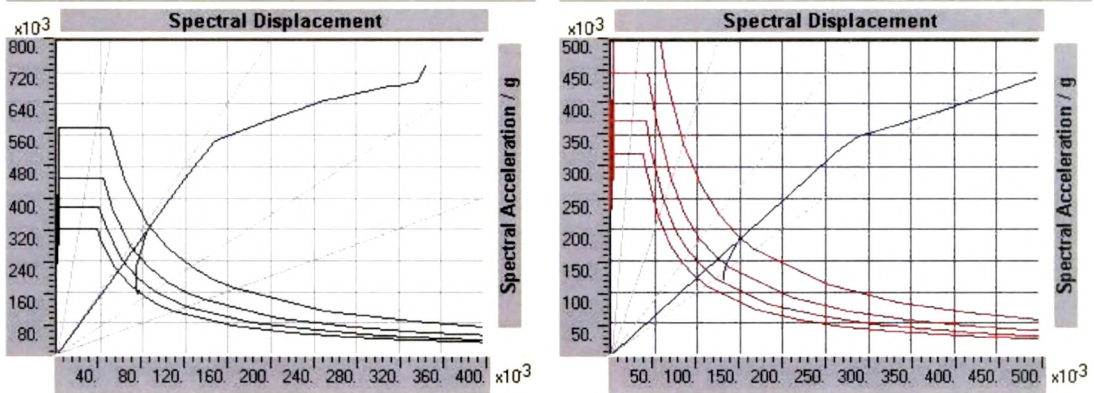


**Fig. 9.26 ADRS Plots – 3000 kNm/rad PX and 1000 kNm/rad PY**

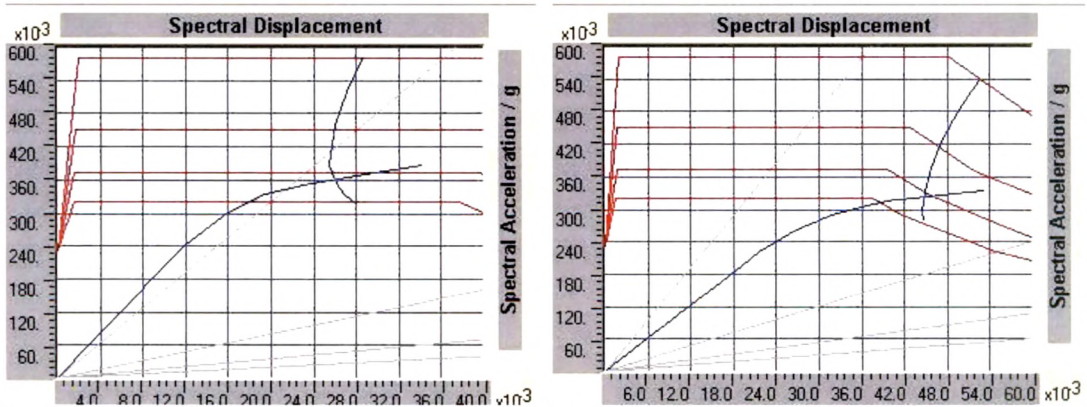


**Fig. 9.27 G+5 Frame ADRS Plots with Full Rigidity under PX and PY**

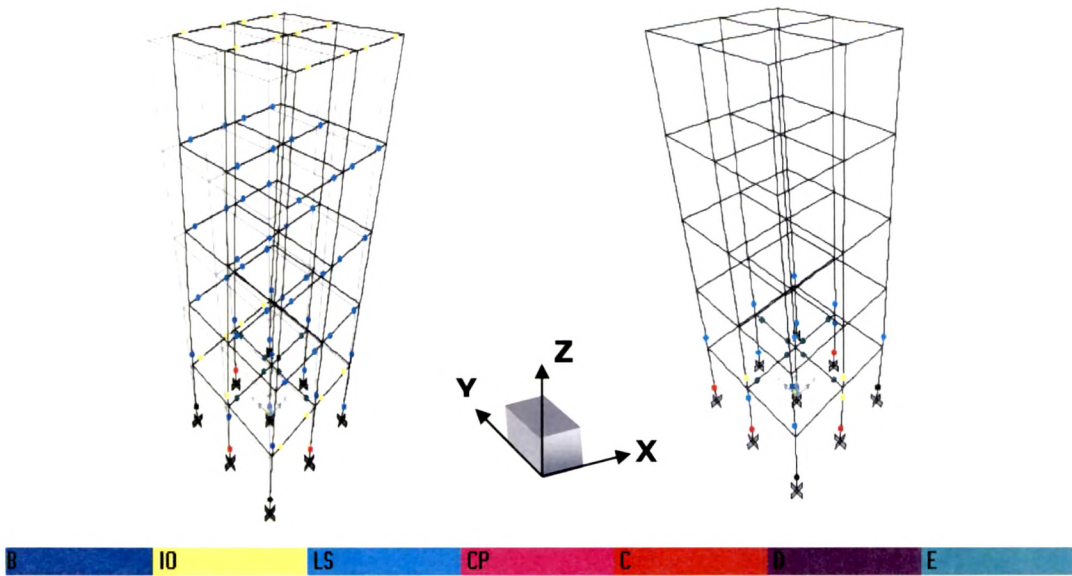


**Fig. 9.28 G+4 Frame with Semirigid Joints under PUSH X and Y**

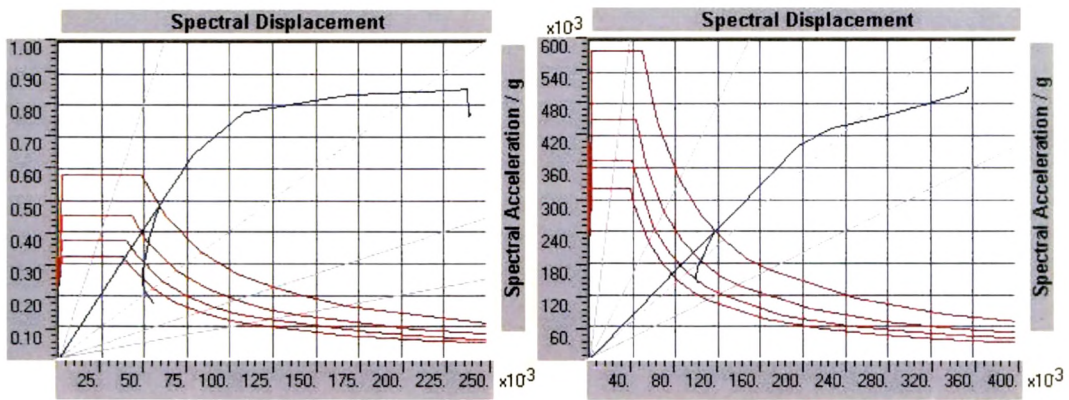


**Fig. 9.29 ADRS Plots – 5000 kNm/rad PX and 1000 kNm/rad PY**

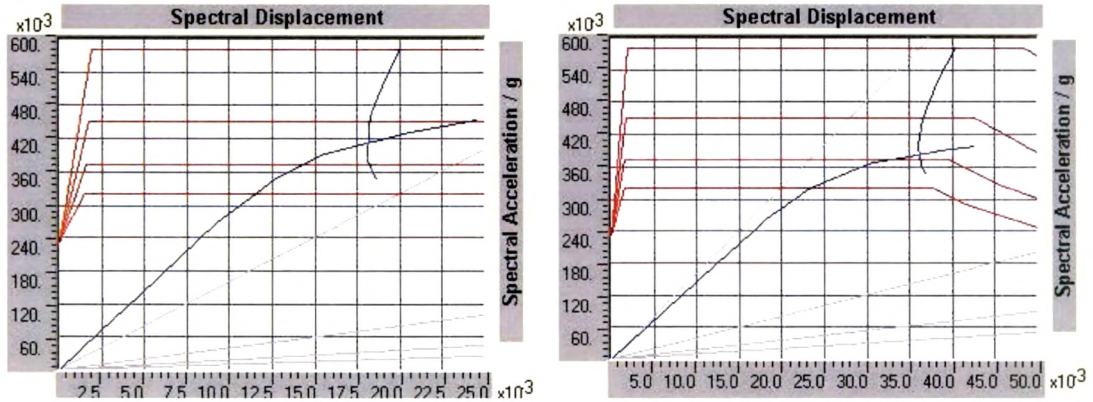


**Fig. 9.30 G+4 Frame ADRS Plots with Full Rigidity under PX and PY**

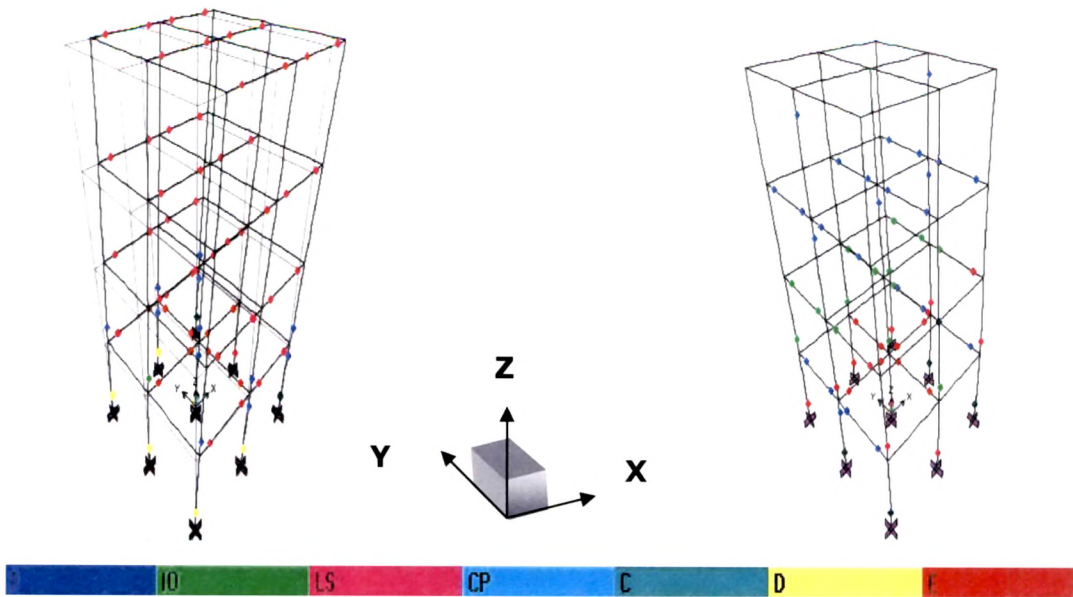


**Fig. 9.31 G+3 Frame with Semirigid Joints under PUSH X and Y**

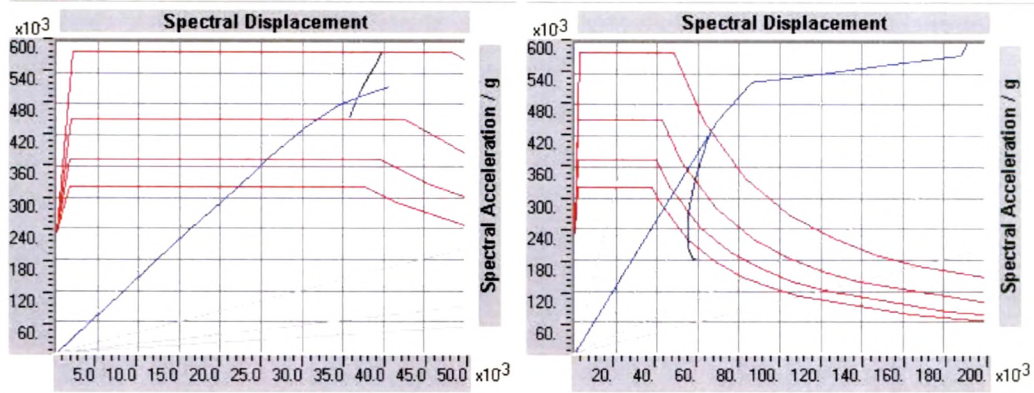


**Fig. 9.32 ADRS Plots – 10000 kNm/rad PX and 3000 kNm/rad PY**

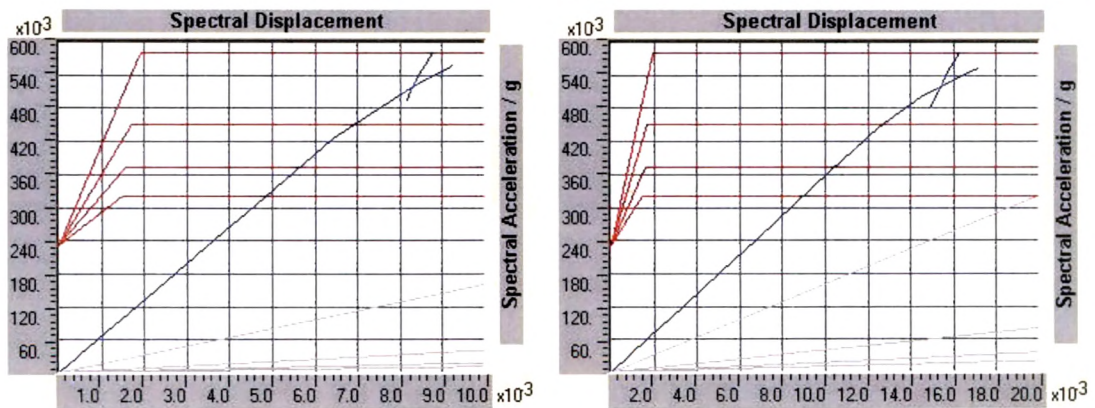


**Fig. 9.33 G+3 Frame ADRS Plots with Full Rigidity under PX and PY**

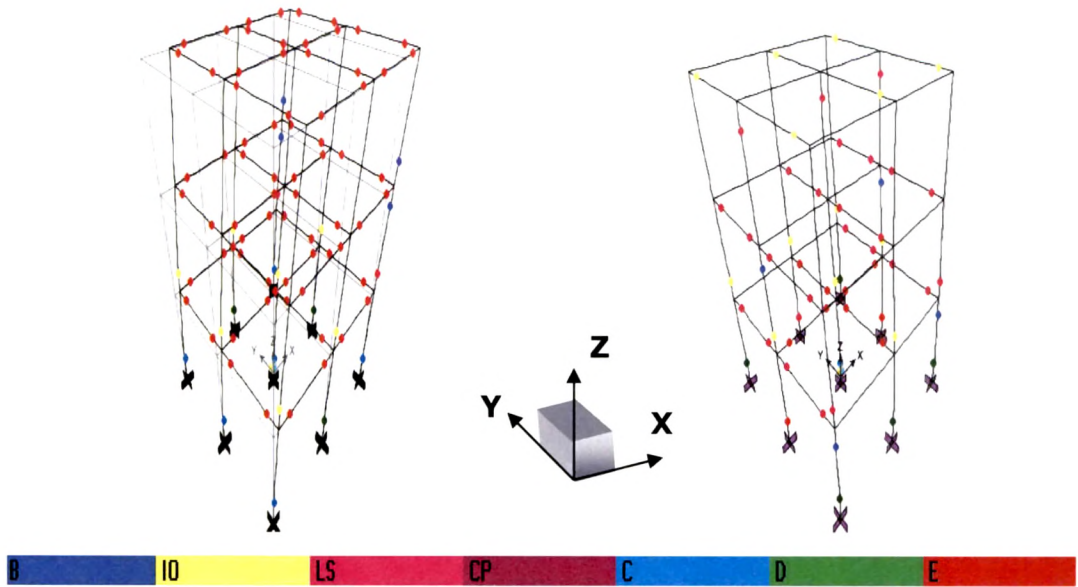


**Fig. 9.34 G+2 Frame with Semirigid Joints under PUSH X and Y**

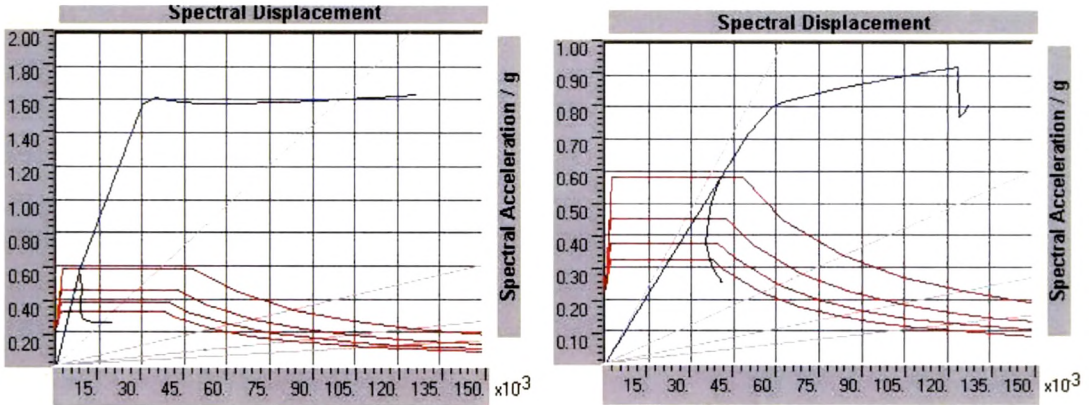


**Fig. 9.35 ADRS Plots – 30000 kNm/rad PX and 7000 kNm/rad PY**

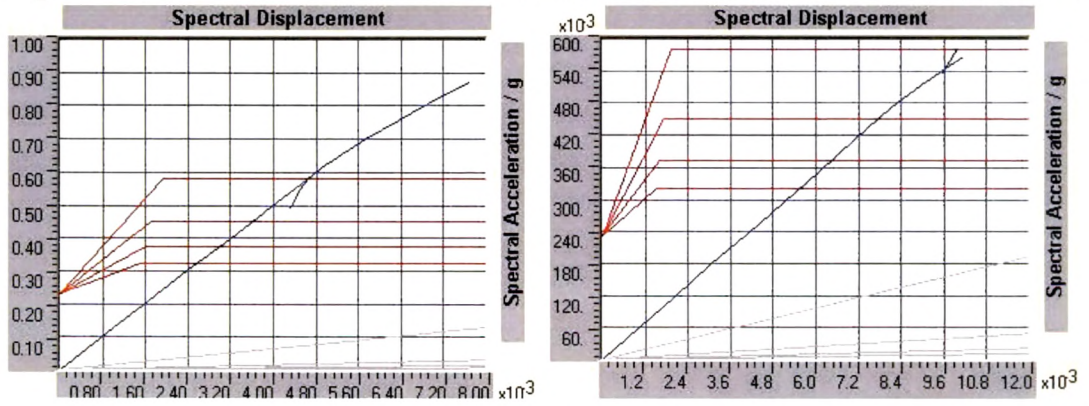


**Fig. 9.36 G+2 Frame ADRS Plots with Full Rigidity under PX and PY**

The results of the pushover analysis for all the frames are presented in a consolidated manner in the form of important parameters noted at performance point. **Table 9.9** presents the roof displacement of the control node at the roof level as  $D$ , the shear force at base as  $V$  at the performance point for push given in the  $X$  direction. The table also notes the Spectral displacement  $S_d$  and the Spectral acceleration  $S_a$  along with effective time period  $T_{eff}$  and the effective damping  $\beta_{eff}$  at performance point. The performance point is represented by the roof displacement versus the base shear plot in **Fig. 9.37** corresponding to **Table 9.9** for each of the frames G+8 to G+2. The performance point due to semi rigid joints and the performance point for fully rigid frame are plotted as the ends of a line in the plot. The similar results for push in the  $Y$  direction are presented in **Table 9.10** and the corresponding plot shown in **Fig. 9.38**. It may be noted here that the joint rigidity at which the peak earthquake moments are observed are different in each of the lateral  $X$  and  $Y$  directions for all the space frame models.

It is worth mentioning here that in all the ADRS plots presented in this chapter, a single demand curve with variable damping is also plotted. It is the intersection of the capacity curve with the single demand curve with variable damping which is defined as the performance point. The fact that as plastic hinges develops in the model, the energy absorbing capacity and thus, the damping, increases. This, in turn, increases the time period of the structure. Hence, in a push over analysis, the effective time period and the effective damping at performance point are different than their initial values.

**Table 9.9 Values at Performance Point for PUSH in X direction**

Storey	Rigidity (kNm/rad)	D (m)	V (kN)	Sd (m)	Sa (g)	Teff (sec)	$\beta_{eff}$ (%)
G+8	Full	0.066	455.31	0.053	0.285	0.866	23.5
	3000	0.218	212.33	0.153	0.147	2.048	8.5
G+7	Full	0.054	367.43	0.043	0.329	0.728	22.5
	2000	0.210	184.85	0.147	0.191	1.758	15.2
G+6	Full	0.043	330.28	0.034	0.387	0.597	20.5
	2000	0.196	144.35	0.121	0.232	1.449	13.2
G+5	Full	0.031	329.64	0.025	0.452	0.467	17.6
	3000	0.121	206.14	0.086	0.324	1.035	13.2
G+4	Full	0.019	317.95	0.015	0.524	0.337	11.7
	5000	0.081	259.30	0.058	0.479	0.701	9.8
G+3	Full	0.012	279.67	0.009	0.560	0.258	7.9
	10000	0.053	169.43	0.041	0.516	0.564	9.8
G+2	Full	0.006	216.63	0.004	0.577	0.179	5.0
	30000	0.011	194.29	0.008	0.582	0.239	5.0

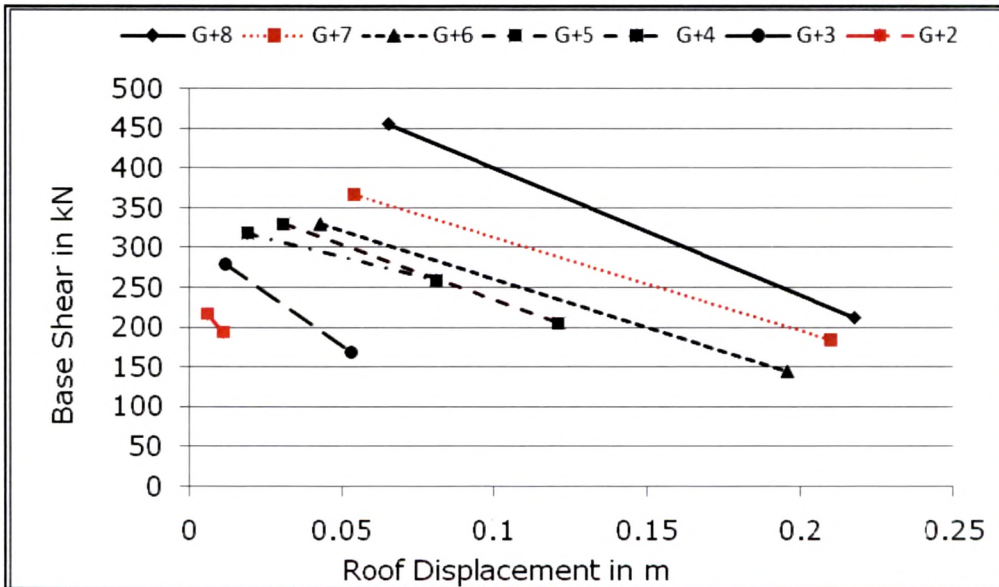


**Fig. 9.37 Performance Points for Semi Rigid and Rigid under Push X**

**Table 9.10 Values at Performance Point for PUSH in Y direction**

Storey	Rigidity (kNm/rad)	D (m)	V (kN)	Sd (m)	Sa (g)	Teff (sec)	βeff (%)
G+8	Full	0.078	403.89	0.064	0.243	1.026	23.4
	1000	0.393	141.85	0.277	0.101	2.779	16.9
G+7	Full	0.066	341.21	0.054	0.298	0.851	22.7
	1000	0.297	129.77	0.209	0.135	1.830	13.9
G+6	Full	0.066	291.09	0.053	0.334	0.802	19.1
	1000	0.259	113.04	0.187	0.150	2.239	9.8
G+5	Full	0.053	294.83	0.043	0.398	0.657	17.6
	1000	0.210	117.45	0.151	0.186	1.809	13.2
G+4	Full	0.042	291.07	0.034	0.459	0.543	14.5
	1000	0.163	124.11	0.117	0.239	1.403	8.5
G+3	Full	0.022	266.47	0.007	0.552	0.354	8.5
	3000	0.087	136.27	0.063	0.440	0.760	7.6
G+2	Full	0.013	210.23	0.010	0.582	0.269	6.4
	7000	0.035	202.40	0.026	0.566	0.426	5.0

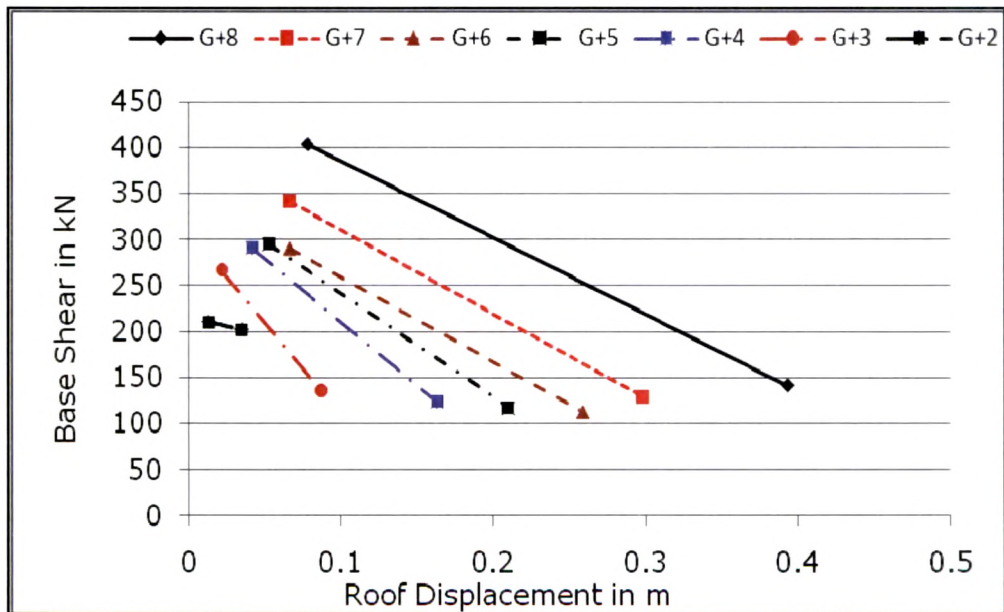


**Fig. 9.38 Performance Points for Semi Rigid and Rigid under Push Y**

## 9.5 OBSERVATIONS AND DISCUSSION OF RESULTS

The analysis of the RC space frames was done in two parts in this chapter. The first part consisted of applying the earthquake load in the two lateral directions for varying joint rigidity and noting down the moments at the left most joint of the beam denoted by points A and B in **Fig. 9.4**. The following points are important to note from the first part of analysis:

1. **Figure 9.2** shows that the moment at the roof level node increases as the joint rigidity increases, attains a peak value and then decreases to that for a fully rigid frame, for earthquake load case. The peak is not observed by varying the joint rigidity for live load case. Peak moment is observed only for lateral load cases and not for gravity loads.
2. **Figure 9.3** indicates that as the joint rigidity increases, the fundamental time period decreases and becomes constant at higher rigidity. Thus, with semi rigid joints, it becomes a ductile structure and attracts less earthquake force as the time period increases.
3. **Tables 9.2 to 9.4** along with **Figs. 9.9, 9.11, 9.13** and **9.15** indicate that as the joint rigidity increases, the moment at A and B at the roof level due to earthquake force in the X and Y directions respectively, increases gradually, reaches a peak value and then decreases to the value of moment observed at the fully rigid joint state.
4. It is also observed that the peak moment beyond the fully rigid moment phenomenon is observed only for the top stories. The difference between the peak moment and the fully rigid moment is highest at the topmost level of a frame. This is indicated by **Tables 9.5** and **9.7** for the X and Y direction force respectively.
5. The ratio of the peak moment to fully rigid moment at the roof level node increases with increase in the number of storey. This is indicated in **Tables 9.6** and **9.8** for the two lateral directions.

6. The ratio of peak moment to the fully rigid moment in a frame is varying from 1.11 for G+2 frame to 2.66 for G+8 frame, which indicates a rise of 238% for earthquake force in the Y direction. For the X direction force this ratio ranges from 1.1 for G+2 frame to 2.39 for G+8 frame which is an increase by 217%.
7. It is also observed that as the number of storey increase, the peak moment is also observed in the storey below the top storey. This is true for G+6, G+7 and G+8 frames for X direction force as seen in **Table 9.6**. The top two storey indicate this peak for G+7 and G+8 frames for force in the Y direction as seen in **Table 9.8**.

The above observations indicate that as the structure displaces in the lateral direction, the bending moment at the roof level node increases beyond the value it would have indicated if all the beams were considered fully rigid. Thus, the bending stress in the hinge at roof level will increase because of semi rigidity. This effect can be studied by subjecting the models to push over analysis considering the rigidity of the beam ends as equal to that which corresponds to the peak moment. The performance point results obtained from the pushover analysis of all the frames formed the second part of the analysis. The following observations are important to note from this part of the analysis.

1. The performance point for fully rigid frames is achieved at higher base shear and lower roof displacement as compared to that for semi rigid frames. This is clear from **Tables 9.9** and **9.10** presented for the push in the two lateral directions.
2. **Figures 9.37** and **9.38** indicate that the performance point difference in the base shear and roof displacement between a frame with rigid joints and semi rigid joints increases with the increase in the number of storey. This trend is observed for push in both the lateral directions.

3. **Tables 9.9** and **9.10** indicate that as the number of storey increases, the effective damping at performance point increases monotonically for fully rigid frames. This trend is observed for both the lateral direction push. The same is not observed for frames with semi rigid joints. The increase in the effective damping is an indication of damage in the frame. Thus, one can say that the damage in the frames increases with the increase in number of storey for an RC frame with fully rigid beam column joints.
4. It can be seen from **Figs. 9.37** and **9.38** that for the G+2 frame, the difference in the performance point between fully rigid frame and semi rigid frame is very small. Thus, it may not be worthwhile studying these frames under earthquake loads.
5. The effective time period at performance point for semi rigid frames is always much higher than that for the same frame with all joints considered as fully rigid. This is clear from **Tables 9.9** and **9.10**.